Geophys. J. Int. (2001) **146,** 813–826

Thermal controls on flexure of underthrust continental lithosphere

C. David Brown

Department of Earth and Planetary Sciences, Washington University, Campus Box 1169, *One Brookings Drive, Saint Louis,* MO 63130–4899.
E-mail: dbrown@wurtzite.wustl.edu

Accepted 2001 May 1. Received 2001 April 10; in original form 2000 August 1

SUMMARY

We model the thermal and mechanical structure of Precambrian foreland lithosphere subject to a range of initial thermal states and evolving thermal perturbations beneath an orogen. Temperatures in the lower crust exert a critical control over the flexural response by regulating crust–mantle decoupling. By careful consideration of crustal heat production and temperature-dependent thermal conductivity, we verify that at least half the surface heat flow in Archean terranes is supplied by the crust and find that Moho temperatures in Proterozoic lithosphere may be as high as 800 K (525 °C). Such 'hot' Precambrian forelands may have an effective elastic thickness of less than 10 km. The ability of crustal heating beneath the orogen to enhance weakening of continental lithosphere is strongly dependent on the convergence rate. A rapidly underthrust foreland is insufficiently heated by thermal diffusion into the zone of maximum lower crustal deformation to significantly modify the flexural signature. This process has a minor effect at the 5 mm year^{-1} or greater convergence rates characteristic of most active orogens, but it may cause a marked reduction in lithospheric strength following the cessation of convergence. We propose that the large, $\sim$10–100 km range of observed mountain belt effective elastic thicknesses can be entirely explained by the known variability of Precambrian surface heat flow, crustal heat generation, rock thermal conductivity, and lithospheric rheology without invoking any other mechanisms.

Key words: continental crust, flexure of the lithosphere, geothermal evaluation, orogeny, plate convergence, rheology

1 INTRODUCTION

The deformation of continental lithosphere is controlled principally by its thermal state. Flexure of lithosphere subject to surface loads (e.g. mountain belts) and subsurface loads (e.g. lateral density variations) is commonly analysed to infer the lithospheric thickness and strength. However, the relationship between thermal and mechanical structure is usually ignored by approximating the lithosphere as an elastic plate and deriving an 'effective elastic thickness' when modelling flexure at forelands and mountain ranges (e.g. Stewart & Watts 1997). Few flexural studies have examined the direct thermal control on the continental lithosphere's rheology (Burov & Diament 1995; Brown & Phillips 2000). For instance, at some mountain belts underthrust Precambrian lithosphere exhibits anomalously low effective elastic thicknesses despite a presumably 'cold' geotherm. This phenomenon has been chiefly attributed to crust–mantle decoupling rather than the thermal state of continental lithosphere (McNutt *et al.* 1988; Watts 1992; Burov & Diament 1995).

We have previously modelled crust–mantle decoupling and found it unable to explain the extremely low ($\sim$10-km) effective elastic thicknesses estimated for some Precambrian forelands (Brown & Phillips 2000). Our prior work examined orogenic loading with a more rheologically rigorous model than earlier studies by using a two-dimensional stress- and time-dependent elastic-viscous-plastic finite element analysis. We investigated the effects of many parameters on the flexural response to mountain belt growth, including a range of geotherms, a variable crustal thickness, different loading rates, alternative boundary conditions (a continuous or broken plate edge), and uncertainties in ductile crustal rheology.

However, there were two important shortcomings in Brown & Phillips (2000) that are addressed in the present paper. First, we assumed a generally unique mapping between crustal age and lithospheric geotherm (following Burov & Diament 1995). Such a relationship is appropriate for oceanic lithosphere but dubious for continental plates. Below we argue that there is substantial variability in the heat flow and heat production of Precambrian crust that is central to the problem of anomalous effective elastic thicknesses. Second, we previously neglected the thermal evolution of the underthrust foreland lithosphere as it heats up by thermal diffusion beneath the orogen. Here

we also examine this potentially significant process. Other improvements of lesser importance include a more realistic load distribution and a laterally advancing (rather than vertically growing) orogen.

1.1 Initial geotherm

Foreland lithosphere underthrust at many young mountain belts, including the Himalaya, Andes, and Carpathians, is Precambrian in age. This lithosphere is assumed to be in thermal steady state by the Cenozoic owing to its prolonged, stable history. The heat flow measured at the surface of Precambrian crust has a large range, but is typically 40–60 mW m^{-2} (Nyblade & Pollack 1993; Pollack *et al*. 1993). This range is observed at the Himalayan, Andean, and Carpathian Proterozoic forelands (Gupta 1993; Roy & Rao 2000; Henry & Pollack 1988; Springer & Förster 1998; Demetrescu & Andreescu 1994). However, the effective elastic thicknesses at these sites range from about 10 km to nearly 100 km (Karner & Watts 1983; Lyon-Caen & Molnar 1983, 1985; Royden 1993a; Lyon-Caen *et al*. 1985; Watts *et al*. 1995; Stewart & Watts 1997; Royden & Karner 1984; Maţenco *et al*. 1997).

Several workers have presented steady-state, one-dimensional, conductive geotherms for continental lithosphere (Pollack & Chapman 1977; Chapman 1986; Rudnick *et al*. 1998). One approach to estimating such geotherms, and the one we adopt, is to take a surface heat flow and extrapolate temperatures at depth given a radiogenic heat production distribution. The two most salient issues in this problem are (1) how does heat production vary with depth in the crust and, less importantly, in the mantle, and (2) what is the depth dependence of thermal conductivity.

1.1.1 Heat production

The favoured parametrization of crustal heat generation with depth is the exponential function, based on an observed linear surface heat flow–heat production relation (e.g. Blackwell 1971; Turcotte & Schubert 1982; pp. 145–148; Jessop 1990). Although such a relation may be appropriate for granitic batholiths, its applicability to continental crust in general is not clear. Deep boreholes have not substantiated an exponential decrease of heat production in the upper $\sim$10 km (Kremenetsky *et al.* 1989; Clauser *et al.* 1997). Heat production depends primarily on lithology, which is varied and complex in the continents. Two-dimensional models of heterogeneous heat source distributions also reproduce the linear surface heat flow–heat production relationship (Furlong & Chapman 1987; Fountain *et al.* 1987). Therefore, assuming an exact, unique, or universal description of the variation of heat generation with depth is not justifiable.

An alternative procedure, which we employ, is to discretize the crust into two or three depth sections, each with a uniform heat production (e.g. Drury 1989; Rudnick *et al*. 1998). Although this simplified crustal structure may result in somewhat less precise temperatures, they are no less accurate than for an equally inexact, continuous heat production distribution. Temperatures at the base of the crust (which have an important control on the mechanical response to loading) are only weakly sensitive to the detailed partitioning of heat generation in a layered crust, provided that the total heat production is unchanged.

For any form of crustal heat production distribution, an essential question is how much heat is generated within the crust and how much is supplied by the mantle. Data relevant to this question are provided by seismic velocities, exposed crustal cross-sections, and crustal and mantle xenoliths that can be used to infer lithospheric composition (Christensen & Mooney 1995; Rudnick & Fountain 1995; McLennan & Taylor 1996; Rudnick *et al*. 1998). The range of estimated average crustal heat generation is $\sim$0.5–1.2 μW m^{-3}, corresponding to crustal contributions to surface heat flow of at least 50 per cent (Rudnick *et al*. 1998). Heat flow from Archean cratons is distinctly lower than from Proterozoic shields, a difference attributable to some combination of lower heat production in and/or lower mantle heat flow below Archean crust (e.g. Nyblade & Pollack 1993; Lenardic 1997).

Rudnick *et al*. (1998) applied additional constraints on Archean craton geotherms by requiring that they intersect the mantle adiabat and by considering mantle xenolith pressure–temperature data. They found that Archean crustal heat production must either be very low ($\sim$0.4 μW m^{-3}), so that it supplies only $\sim$40 per cent of the surface heat flow, or the xenolith data represent a transient, elevated heat flow. Their estimated temperature at the base of the Archean crust is $\sim$700 K. Other estimates of basal temperatures for Precambrian crust are $\sim$600–800 K (Morgan 1984; Chapman 1986; Jessop 1990). These theoretical geotherms are consistent with geothermobarometry of granulite xenoliths and terranes that implies maximum lower crustal temperatures in shields of $\sim$1100 K (Rudnick 1992; Mezger 1992).

1.1.2 Thermal conductivity

Another important control on theoretical geotherms is the dependence of thermal properties—including conductivity and diffusivity (or specific heat)—on state variables, particularly temperature and pressure. The depth dependence of thermal conductivity has been incorporated in some continental geotherm calculations (e.g. Chapman 1986), and modelling has shown that the temperature dependence of physical properties can be important for the thermal and mechanical evolution of the lithosphere (Ketcham *et al*. 1995; Doin & Fleitout 1996; Starin *et al*. 2000). In addition, recent studies have advanced our understanding of the variability of thermal conductivity.

Thermal conductivity is strongly temperature dependent, decreasing by about a factor of 2 over the range of mechanical lithosphere temperatures ($\sim$275–1000 K) for some rocks. Conductivity is only weakly pressure dependent, increasing no more than $\sim$10 per cent at high confining pressures (Clauser & Huenges 1995). Although rocks have different conductivities according to their mineralogies, the temperature dependence of most crustal materials is similar, and a universal conductivity–temperature function was suggested by Sass *et al*. (1992). Empirical conductivity–temperature functions for a variety of igneous and metamorphic crustal rocks have been published by Zoth & Haenel (1988), Arndt *et al*. (1997), and Seipold (1998). Chapman (1986) and Rudnick *et al*. (1998) modelled a lower crust with a very weakly temperature-dependent conductivity ($\sim$2.6 W m^{-1} K^{-1}), contrary to experimental results for granulite and other metamorphic rocks typical of the middle and lower crust.

Also, Hofmeister (1999) recently derived an improved theory for mineral thermal conductivities with applications to heat

transport in the mantle. Most earlier geotherm models utilized the olivine conductivity function of Schatz & Simmons (1972); Hofmeister's (1999) results differ in two significant respects. First, thermal conductivity is higher (by up to $\sim$20 per cent) at lithospheric temperatures. Second, radiative conductivity is negligible below $\sim$2000 K; hence thermal conductivity is about half the Schatz & Simmons (1972) value at 2000 K. These differences have important implications for mantle geotherms.

1.2 Thermal evolution

Studies of flexure at several mountain belts have indicated that the effective elastic thickness decreases from the foreland toward and beneath the orogen (Lyon-Caen & Molnar 1985; Snyder & Barazangi 1986; Zoetemeijer *et al.* 1990; Stewart & Watts 1997). This horizontal reduction in the flexural rigidity might be explained by increased bending curvatures and/or an actual rheological weakening, perhaps induced by conductive heating of the underthrust plate. Thermal modification of the lithosphere beneath the orogen might also explain the anomalously low elastic thicknesses determined for some Proterozoic forelands.

Previous work has examined the large-scale thermal history of orogens (Chery *et al.* 1991), often using simplified kinematic models (e.g. Batt & Braun 1997; Midgley & Blundell 1997; Henry *et al.* 1997). Also, both steady-state and transient heat transfer models of the orogenic wedge overriding the foreland have been developed (Molnar & England 1990; Royden 1993b; Huerta *et al.* 1998). The latter models demonstrated the importance of erosion and vertical accretion, in addition to volumetric heat production, to the thermal evolution of mountains. They did not include heat transfer between the underthrust plate and orogenic wedge. None of the above studies considered the effects of the orogenic thermal evolution on the mechanical (i.e. flexural) state of the foreland.

Several workers have modelled thermal blanketing of the continental lithosphere by sedimentation, particularly for subsidence and flexure at rift basins (e.g. Stephenson *et al.* 1989; Karner 1991). This process raises the surface temperature of the lithosphere (i.e. at the base of the basin infill); the low thermal conductivity of porous, uncompacted sediments results in a high temperature gradient at shallow depths. Thermal blanketing has also been evaluated for foreland basins by Lavier & Steckler (1997). Their one-dimensional model showed that basin infill could significantly aid crust–mantle decoupling by raising lower crustal temperatures in the steady-state limit. However, this model neglected the spatial and temporal aspects of the heat transfer and mechanical problems for an active orogen. The convergence rate and occurrence of lateral conduction must impose important restraints on the coupled rheologic response of the lower crust.

Transient heat flow depends on the lithospheric thermal diffusivity. Although constant diffusivity is conventionally assumed in theoretical modelling, like conductivity, it is a temperature-dependent property. Empirical data on thermal diffusivity of crustal rocks indicates a decrease of at least 50 per cent between 300 K and 1000 K (Durham *et al.* 1987; Arndt *et al.* 1997). Thermal diffusivity of the mantle can be derived from published thermal conductivity and heat capacity functions for olivine (Gillet *et al.* 1991; Saxena & Shen 1992; Hofmeister 1999).

2 METHODOLOGY

2.1 General approach

In this study we perform both thermal and mechanical modelling of continental lithosphere. The thermal modelling is concerned first with establishing a reasonable range of steady-state geotherms for Precambrian lithosphere and second with the thermal evolution of lithosphere underthrust beneath an orogen. The mechanical modelling determines the flexural response of the lithosphere to loading under these various thermal scenarios. Thus, our complete modelling procedure consists of four steps.

(1) We evaluate a one-dimensional, steady-state, initial lithospheric geotherm given a specified surface heat flow (q_0) and crustal heat production (A_c).

(2) We run a mechanical model with the steady-state geotherm given a particular orogenic wedge advance rate (v).

(3) We model the 2-D heat transfer problem in the foreland lithosphere subject to a changing surface temperature boundary condition (at the interface between the orogenic wedge and the underthrust plate). This temperature depends on the vertical surface deflections beneath the load.

(4) We obtain a second mechanical solution to the flexural problem, replacing the constant geotherm with the transient temperature field.

All modelling is performed with the commercial finite element software MARC, version K7 (MARC Analysis Research Corporation, Palo Alto, California). The details of the elastic–viscous–plastic mechanical modelling were described by Brown & Phillips (2000). Differences, notably in the geotherms and manner of orogenic loading, are explained below. A schematic view of the models is presented in Fig. 1; all model parameters are listed in Table 1.

The lithospheric structure consists of three layers in both the thermal and mechanical models. The upper granitic and lower granulite crust are both 20 km thick; the upper mantle is represented by a dunite composition. The crustal thickness is kept constant at 40 km.

2.2 Steady-state thermal model

Surface heat flow is the primary variable in the steady-state 1-D thermal models; the crustal heat production is a secondary free parameter. The average crustal heat production is $A_c = \frac{1}{2}(A_1 + A_2)$, and the contribution of crustal heat generation to the surface heat flow is $(q_0 - q_c) = A_c h_c$. In the nominal models, $A_c = 0.725$ μW m^{-3} and $A_c h_c = 29$ mW m^{-2}. The boundary conditions to these models are the surface temperature (T_0) and the basal heat flow,

$$q_m = q_o - A_c h_c - A_3(h_m - h_c)\,. \quad (1)$$

We employ the thermal conductivity – temperature functions of Seipold (1998) for granite and granulite and Hofmeister (1999) for olivine. Of particular interest is the temperature at the base of the crust (T_c) resulting from these heat transfer solutions.

Table 1. Thermal–mechanical model parameters and variables.

Parameter	Definition	Value
A_1	heat production, upper crust	1.25 μW m^{-3}
A_2	heat production, lower crust	0.20 μW m^{-3}
A_3	heat production, upper mantle	0.02 μW m^{-3}
C	cohesion	10 MPa
$C_p(T)$	specific heat	—
D	flexural rigidity	—
E_e	Young's modulus, elastic plate	100 GPa
E_1	Young's modulus, upper crust	50 GPa
E_2	Young's modulus, lower crust	75 GPa
E_3	Young's modulus, upper mantle	150 GPa
F_o	net force of orogenic load	—
g	gravitational acceleration	9.8 m s^{-2}
h_c	crustal thickness	40 km
h_e	effective elastic thickness	—
$\overline{h_e}$	laterally averaged effective elastic thickness	—
h_e^{min}	minimum effective elastic thickness (x = 0)	—
h_m	thickness of mechanical lithosphere	—
h_o	maximum height of orogenic wedge	3.5–5.0 km
$h'_o(x, t)$	height of orogenic wedge	—
$k(T)$	thermal conductivity	—
q_0	surface heat flow	40–50 mW m^{-2}
q_c	Moho heat flow	—
q_m	heat flow at the base of mechanical lithosphere	—
t	time	—
T_0	absolute land surface temperature	275 K
$T'_o(x, t)$	lithospheric surface temperature boundary condition	—
$T_c(x, t)$	Moho temperature	—
ΔT_c^{max}	maximum Moho temperature change (x = 0)	—
ΔT_c^{ε}	Moho temperature change at maximum creep strain	—
T_m	temperature at the base of mechanical lithosphere	~1000 K
v	orogenic wedge advance rate	2–10 mm year^{-1}
$w(x, t)$	vertical flexural displacement	—
w_0	vertical displacement at origin	—
x_b	distance between wedge toe and flexural bulge	—
x_o	location of orogenic wedge toe	—
ε_e^c	maximum creep strain in lower crust	—
θ	orogenic wedge surface slope	2°
$\kappa(T)$	thermal diffusivity	—
μ	coefficient of friction	0.7
ν	Poisson's ratio	0.25
ρ_1	density of upper crust	2700 kg m^{-3}
ρ_2	density of lower crust	2900 kg m^{-3}
ρ_3	density of upper mantle	3300 kg m^{-3}
ρ_o	density of orogenic wedge	2600 kg m^{-3}
ρ_w	pore fluid density	1000 kg m^{-3}
$\sigma_o(x, t)$	orogenic wedge load	—
∇T_o	orogenic wedge geotherm	20 K km^{-1}

2.3 Mechanical models

The orogenic advance rate is the primary variable in the 2-D mechanical models. The load is described by a wedge of uniform density (ρ_o) with a specified surface slope (θ) and maximum height above the datum (h_o) that moves at a constant convergence rate (v). This shape is maintained in a self-similar manner as the load advances and grows, but the orogenic wedge also fills in the area of the flexural depression below the datum. At any given time (t) the load height above the datum is

$$h'_o(x) = \min \begin{cases} h_o \\ (x_o - x)\tan\theta \end{cases} \quad (2)$$

where $x_o = vt$. Hence, the applied load is

$$\sigma_o(x) = \rho_o g[h'_o(x) + w(x)], \quad (3)$$

where $w(x)$ is the vertical flexural displacement (positive down). The net force per unit out-of-plane length exerted by the load is then

$$F_o = \int_0^{x_o} \sigma_o(x)dx. \quad (4)$$

We run our models to a total convergence of $x_o = 200$ km because this is the maximum width of underthrust lithosphere

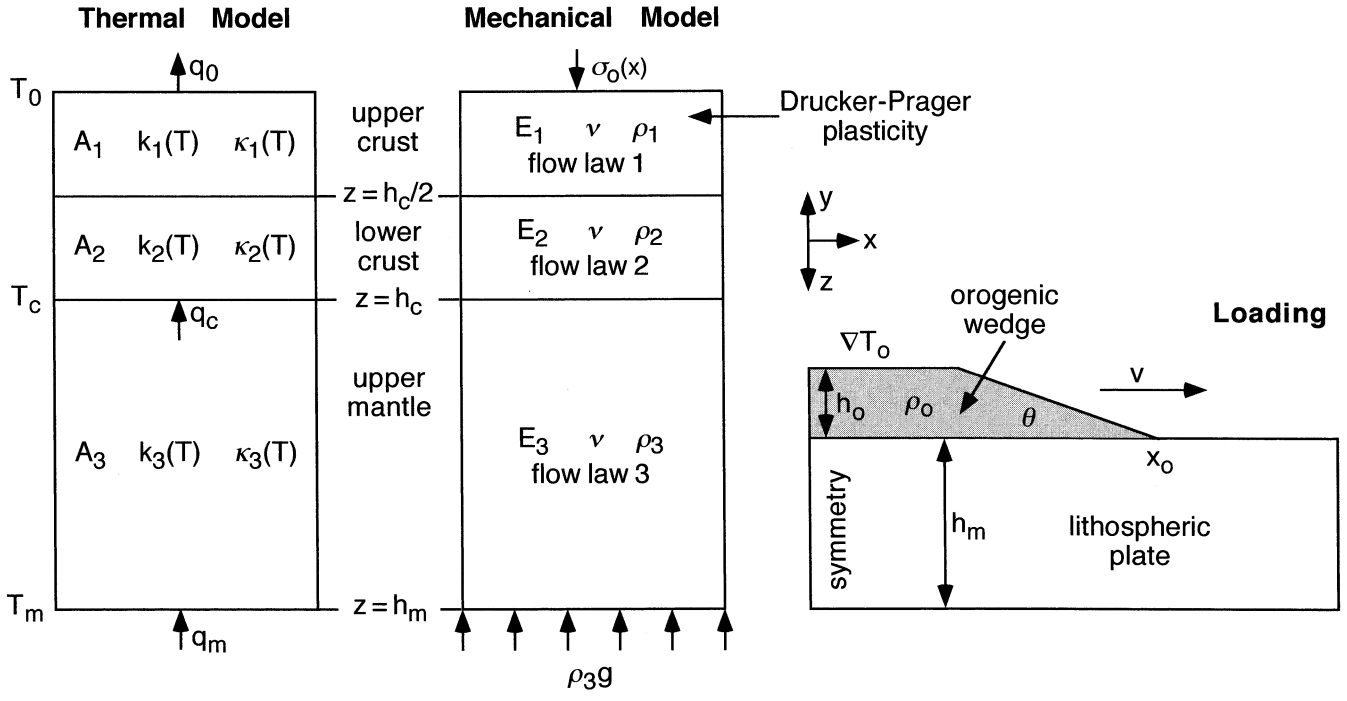

Figure 1. Diagram illustrating thermal and mechanical finite element models. See Table 1 for parameter definitions. Boundary conditions consist of T_0, q_m, σ_o, $\rho_3 g$, and edge symmetry. The orogenic wedge (shaded) is not a physical component of the models; rather, it is represented by the surface temperature ($T_0(x, t)$) and load ($\sigma_o(x, t)$) boundary conditions.

inferred to flexurally support the orogenic load at most mountain belts (e.g. Lyon-Caen & Molnar 1985; Royden 1993a; Stewart & Watts 1997).

The elastic–viscous–plastic (EVP) model rheology is similar to that of Brown & Phillips (2000). Brittle failure is represented by a stress-dependent Drucker–Prager plastic yield criterion and power-law creep by temperature-dependent Maxwell visco-elasticity. The empirical flow laws used are dry Westerly granite for the upper crust (Hansen & Carter 1983), Adirondack granulite for the lower crust (Wilks & Carter 1990), and wet Anita Bay dunite for the mantle (Chopra & Paterson 1981). Boundary conditions consist of symmetry displacement constraints on the left and right edges (i.e. a continuous plate), restoring forces at the base, and orogenic loading at the surface of the lithosphere.

2.4 Coupled thermal–mechanical model

The two-dimensional heat transfer model evaluates the thermal effects of the overriding orogen only (the relatively small volume of foreland basin sediments is ignored). The basal heat flow boundary condition is maintained, but the surface temperature boundary condition varies with distance and time depending on the local thickness of the orogen. ('Surface temperature' hereafter refers to the top of the modelled mechanical lithospheric plate, not the actual land surface.) The surface temperature is calculated in the simplest manner possible: we assume a constant, uniform, linear geotherm in the orogenic wedge. The variable temperature at the surface of the lithosphere at any given time is

$$T_0'(x) = T_0 + [h_o'(x) + w(x)]\nabla T_o \,. \tag{5}$$

The value chosen for this gradient, $\nabla T_0 = 20$ K km^{-1}, is at the upper end of the steady-state, near-surface wedge geotherms determined by Huerta *et al.* (1998). Because the thermal gradient is initially lower and decreases with depth, our approach overestimates the likely temperature boundary condition. Therefore, we are maximizing the thermal and flexural influence of orogenic heating on the underthrust plate.

Heat transfer from the surface into the lithosphere is controlled by the thermal diffusivity, which is defined as

$$\kappa = k/\rho C_p \,. \tag{6}$$

The specific heat at constant pressure (C_p) is the property required by MARC. We employ the temperature-dependent diffusivity functions of Durham *et al.* (1987) for Stripa granite 2 (upper crust) and Creighton gabbro (lower crust), and the temperature-dependent heat capacity of Gillet *et al.* (1991) for forsterite (upper mantle). The diffusivity functions for the crust are combined with temperature-dependent thermal conductivity (Section 2.2) to calculate C_p.

The EVP mechanical model is run under the same conditions as before, but now temperatures vary spatially and with time. (This is not a truly coupled model because the heat transfer and stress solutions are obtained separately.) The hotter crustal temperatures result in a weaker rheology and a greater flexural displacement. Because we maintain a constant load height above the datum (h_o), the orogenic root is deeper and the net load acting on the plate is slightly greater than for the constant lithospheric geotherm model.

2.5 Elastic plate solution

The effective elastic thickness (h_e) is a useful parameter for characterizing the synthetic EVP flexural profiles and for comparing these models to flexural results at real-world mountain belts. However, h_e cannot be uniquely determined because it

depends on the elastic plate model used (e.g. continuous or broken), the free parameters chosen, what part of the data or synthetic model it is fit to, and whether the data comprise surface deflections or gravity (Moho deflections) (Brown & Phillips 2000). We consider two alternatives for evaluating h_e.

First, the Fourier transform of the flexure equation,

$$D\frac{d^4w}{dx^4} + \rho_3 g w(x) = \sigma_o(x), \tag{7}$$

yields an analytic solution with one free parameter, the flexural rigidity (D):

$$W(k) = \frac{S(k)}{(Dk^4 + \rho_3 g)} \tag{8}$$

where $W(k)$ and $S(k)$ are the real Fourier transforms of the EVP model surface displacements (w) and the applied EVP model load (σ_o), k is the wavenumber, and

$$D = \frac{E_e h_e^3}{12(1-\nu^2)}. \tag{9}$$

This method gives a representative, average effective elastic thickness for the EVP solutions ($\overline{h_e}$) via a non-linear least squares fit of eq. (8).

Second, we estimate the laterally variable effective elastic thickness with a finite difference solution of the flexure equation (after Mueller & Phillips 1995). This more involved elastic fit is necessary because many studies at mountain belts have included and required a hinterland-decreasing effective elastic thickness (Section 1.2). A Gaussian function is used to represent the flexural rigidity:

$$D(x) = D_\infty - \Delta D \exp\left(-\frac{x^2}{b^2}\right). \tag{10}$$

This is a convenient description of decreasing flexural rigidity toward and beneath the orogen. The EVP model load is applied to the elastic plate, and D_∞, ΔD, and b are the free parameters that are determined. We minimize the misfit relative to the synthetic model surface displacements using Powell's method (Press *et al.* 1992; pp. 412–420). This technique is sensitive to the starting values of the free parameters, so we obtain fits with a range of starting values and search for the smallest misfit. We characterize the resulting elastic solution by the minimum $h_e(x)$ at the load axis, $x=0$ (h_e^{min}).

3 RESULTS

3.1 Steady-state Precambrian geotherms

Our approach to modelling and evaluating Precambrian geotherms closely follows that of Rudnick *et al.* (1998). We consider two situations: Archean cratons with $q_0 = 40$ mW m^{-2} and Proterozoic shields with $q_0 = 40$–50 mW m^{-2}. We assign a relatively low heat production of 0.02 μW m^{-3} to the upper mantle, compatible with the estimated heat generation of alkali basalt peridotite xenoliths (Rudnick *et al.* 1998). We compare the model geotherms to cratonic peridotite pressure–temperature data and a likely mantle adiabat.

3.1.1 *Archean cratons*

For Archean lithosphere, we compute geotherms with $A_c = 0.4$–0.7 μW m^{-3}, or an integrated crustal heat production that contributes 40–70 per cent of the surface heat flow. Heat generation within the crust is partitioned such that 77 per cent of the crustal heat flow is supplied by the upper crust and 23 per cent by the lower crust ($A_1/A_2 = 3.3$), comparable to Rudnick *et al.* (1998). These geotherms are plotted in Fig. 2(a).

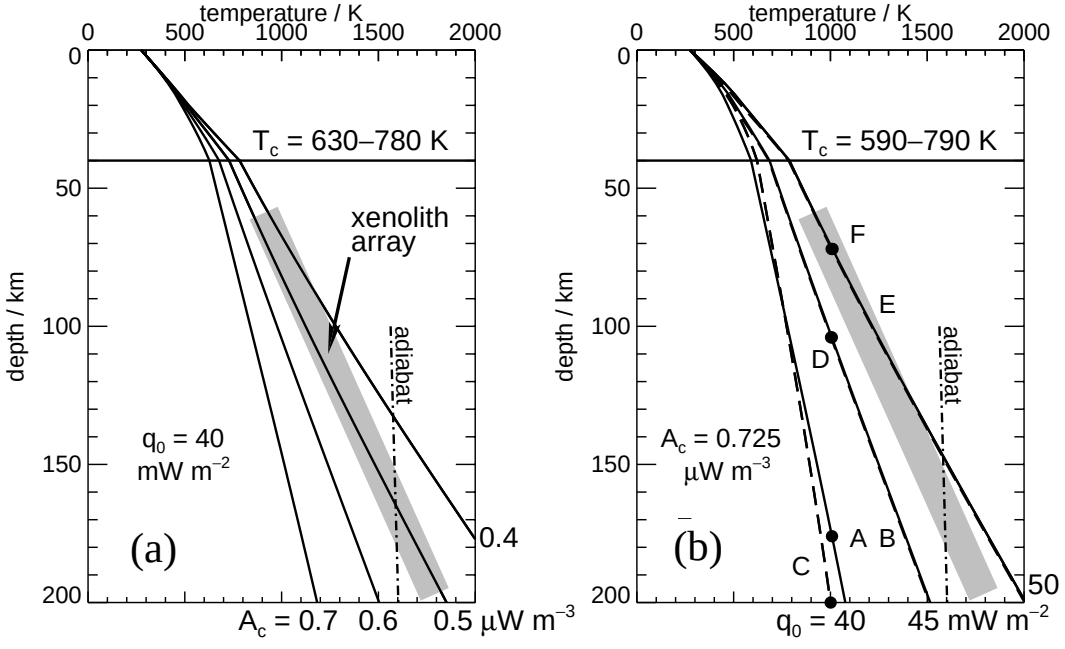

Figure 2. Steady-state geotherm results. The shaded zone of xenolith geothermobarometry data and the mantle adiabat are after Rudnick *et al.* (1998). (a) Archean lithosphere geotherms, with a surface heat flow of 40 mW m^{-2}. The four geotherms correspond to different assumed average crustal heat production values; $A_c = 0.5$ μW m^{-3} best matches the xenolith data. (b) 'Proterozoic' geotherms used in mechanical models for an assumed crustal heat production of 0.725 μW m^{-3}. The three solid lines correspond to different surface heat flows; the dashed line, for $q_0 = 45$ mW m^{-2}, corresponds to a higher value of A_c (Table 2). Geotherms B and E are almost identical to D and F. The dots mark the base of the mechanical lithosphere ($z = h_m$).

The Archean geotherm results are similar to those of Rudnick *et al.* (1998), with two notable exceptions. First, temperatures in the lower crust are higher for a given A_c, a direct consequence of the greater sensitivity of granulite thermal conductivity to temperature (Section 1.1.2). The difference is about 60 K ($A_c = 0.4$ μW m^{-3}) or almost 10 per cent. Second, the mantle temperature gradient is more linear and less curved, reflecting the minimal contribution of radiative conductivity in olivine at these temperatures (Hofmeister 1999).

A consequence of these two effects is that lithospheric temperatures at all depths are hotter for a given A_c than calculated by Rudnick *et al.* (1998). We obtain good agreement with xenolith pressure–temperature data at $A_c = 0.5$ μW m^{-3}. This value is higher than their 0.4 μW m^{-3} and more in line with expectations that the crust supplies at least 50 per cent of surface heat flow. Rudnick *et al.* (1998) noted that the xenolith data may represent equilibration at a much earlier time under conditions of higher heat flow, allowing a greater crustal heat production. If $A_c = 0.7$ μW m^{-3}, the xenolith data are matched for $q_0 \approx 47$ mW m^{-2}. The more linear mantle geotherm also results in a thinner Archean thermal lithosphere (defined by the intersection of the geotherm with the adiabat): 165 km for $A_c = 0.5$ μW m^{-3} and 370 km for $A_c = 0.7$ μW m^{-3}. Hofmeister's (1999) conductivity–temperature function does not significantly alter Rudnick *et al.*'s (1998) finding that the mantle heat production must be relatively low for Archean geotherms to converge with the adiabat.

3.1.2 *Proterozoic shields*

A second set of 'Proterozoic' geotherms is utilized in our mechanical modelling. These geotherms encompass a range of heat flow and crustal heat production (Table 2). Heat flows of 40–50 mW m^{-2} represent measurements of foreland lithosphere at several mountain belts of interest (Section 1.1). A representative average crustal heat production for Proterozoic or bulk crust is no better known—but may be higher—than for Archean crust. Estimates range from 0.6 to 1.1 μW m^{-3} (Rudnick *et al.* 1998), and we take $A_c = 0.725$ μW m^{-3} as a nominal value. This fairly low average crustal heat production may be more typical of Precambrian than bulk crust and is conservative in the sense that it forces temperatures in the lower crust to be relatively high. The corresponding contribution of the crust to surface heat flow is 29 mW m^{-2}, in agreement with the conclusions of McLennan & Taylor (1996).

Several Proterozoic geotherms are plotted in Fig. 2(b). Note that at $q_0 = 40$ mW m^{-2} the Proterozoic geotherm is paradoxically cooler than the Archean geotherms. This peculiarity is attributable to the relatively lower Proterozoic mantle heat flow that compensates for the additional crustal heat generation.

Table 2. Geotherm models.

Model	q_0 (mW m^{-2})	A_c (μW m^{-3})	T_c (K)	h_m (km)
A	40	0.725	590	176
B	40	0.6	682	104
C	45	0.9	621	200
D	45	0.725	685	104
E	45	0.6	784	72
F	50	0.725	788	72

A Proterozoic surface heat flow of ~50 mW m^{-2} is required to attain similar lithospheric temperatures as the preferred 40 mW m^{-2} Archean geotherm. Therefore, if a compositional (and heat production) difference does exist between Archean and Proterozoic crust, Proterozoic lithosphere may be locally cooler and stronger than Archean lithosphere with the same surface heat flow.

3.2 Mechanical models

For the purely mechanical models we consider a range of geotherms (Table 2, Fig. 2b) and convergence rates. Selected results of these models are listed in Table 3 and are shown in Figs 3 and 4. These figures illustrate the surface displacements of the EVP solutions beneath and near the load. Also plotted are the best fit elastic plate solutions and $h_e(x)$ for the variable flexural rigidity model.

The geotherm exerts the strongest control on the lithospheric flexural response, as has previously been recognized. For the same rheology and loading conditions (i.e. v, t, and x_o), increasing the surface heat flow by just 5 mW m^{-2} yields substantially different flexural signatures (Fig. 3a). Corresponding increases in the maximum deflection and decreases in the effective elastic thickness are of order 70 per cent. For these representative Precambrian lithospheric geotherms and orogenic loading scenarios, a range of elastic thicknesses (h_e^{min}) of 100 km down to 10 km is entirely feasible—even without any heat transfer from the orogen included (e.g. models A1 and F1, Fig. 3b). Decreasing crustal heat production from $A_c = 0.725$ μW m^{-3} to an acceptable 0.6 μW m^{-3} has roughly the same effect on the geotherm as increasing q_0 by 5 mW m^{-2} (e.g. compare geotherms D, E, and F in Table 2 and Fig. 2b). Therefore,

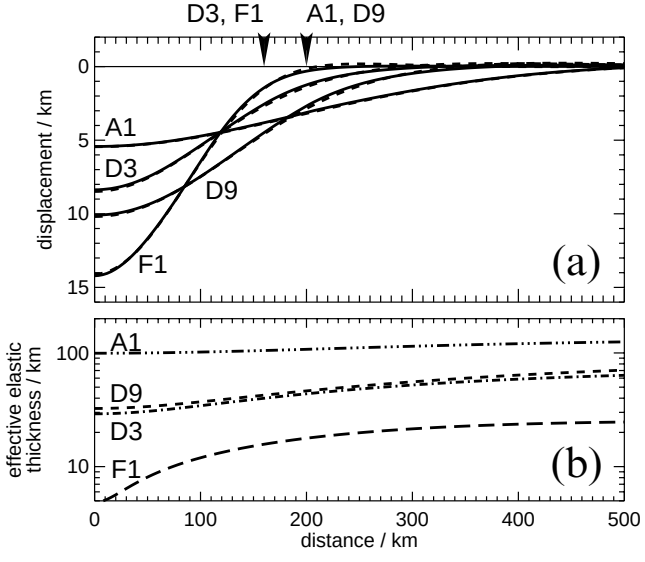

Figure 3. Finite element model flexural results for different geotherms, showing (a) vertical surface displacements and (b) laterally variable effective elastic thicknesses. Arrows mark locations of the orogenic wedge toe (x_o) at this time in model evolution. The dashed curves in the top panel show the best fit elastic plate displacements. Compare models A1 and D9 (40 and 45 mW m^{-2}) and models D3 and F1 (45 and 50 mW m^{-2}), which illustrate the 10–100 km range of effective elastic thicknesses obtainable with appropriate Proterozoic geotherms. See Table 3.

Table 3. Mechanical model results.

Model	v (mm yr^{-1})	t (Myr)	x_o (km)	F_o (TN m^{-1})	w_0 (km)	ε_e^c (per cent)	$\overline{h_e}$ (km)	h_e^{min} (km)	Fig.
A1	10	20	200	40	5.4	0.10	108	99	3
A2	10	40	400	156	16.5	0.34	90	79	
B1	10	20	200	61	12.8	19	40	33	
C1	5	40	200	29	3.7	0.27	119	106	
D0	0	40	200	52	10.8	19	36	—	
D1	2	40	80	5.2	1.3	1.8	59	46	
D2	2	60	120	17	4.4	9.1	43	34	
D3	2	80	160	34	8.4	17	36	29	3
D4	2	100	200	53	11.5	22	32	25	
D5	5	10	50	1.5	0.33	0.09	77	48	4
D6	5	20	100	9.4	2.3	3.1	57	43	4
D7	5	30	150	28	6.6	12	43	34	4
D8	5	40	200	51	10.7	18	36	28	4
D9	10	20	200	49	10.1	15	41	32	3
E1	2	80	160	43	13.8	40	13	5	
E2	2	100	200	60	16.0	42	13	0	
F1	2	80	160	44	14.2	43	11	0	3

For all models $h_o = 3.5$ km, except A1 and A2 for which $h_o = 5$ km.

uncertainties in crustal heat generation allow even lower effective elastic thicknesses for the same surface heat flows (cf. models E2, D4 in Table 3).

The change in the flexural signature with time and hence load magnitude is depicted in Fig. 4 (models D5–8). The surface subsidence and effective elastic thickness vary non-linearly with time owing to the non-linear rheological response and the changing load geometry. Note how the increasing maximum effective creep strain in the lower crust (ε_e^c) correlates with the maximum subsidence (w_0) and inversely with the elastic thickness (Table 3).

The loading rate has a minimal effect on the flexural behaviour (models D4, D8, D9). Although a higher convergence rate increases strain rates, thereby reducing the effective viscosity and Maxwell viscoelastic relaxation time (via the flow law), we find that the relaxation time decreases somewhat less than the characteristic loading time does. Thus, the overall flexural response should be stiffer because bending stresses are relaxed slower than they accumulate. This behaviour is especially apparent in the decreasing maximum deflections, decreasing maximum lower crustal creep strains, and increasing effective elastic thicknesses with increasing convergence rate. However, all three models (D4, D8, D9), as well the one with zero convergence rate (i.e. the load just grows vertically with x_o fixed, model D0), display very similar flexural profiles at $x_o = 200$ km.

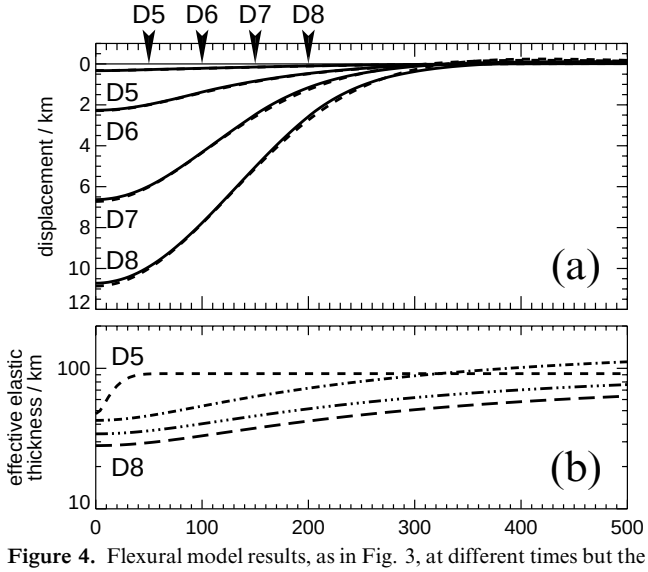

Figure 4. Flexural model results, as in Fig. 3, at different times but the same geotherm and loading rate. Models D5–8 correspond to times of 10, 20, 30, and 40 Myr with a 45 mW m^{-2} surface heat flow.

3.3 Coupled thermal–mechanical models

3.3.1 Heat transfer

Fig. 5 shows the change in temperature relative to the original steady-state geotherm for a typical model (D8b). The maximum change in the surface temperature boundary condition is $\sim$280 K ($w_0 + h_o = 14$ km, $\nabla T_o = 20$ K km^{-1}), but naturally temperature changes are much less within the lithosphere owing to the time required for heat to diffuse deeper. We refer to the maximum temperature change at the Moho (ΔT_c^{max}), which occurs at the load axis ($x = 0$), as well as the temperature change at the location of maximum lower crustal creep strain in the purely mechanical model (ΔT_c^{ε}). The change in Moho temperature as a function of time and convergence rate is plotted in Figs 6 and 7; ΔT_c for all models is provided in Table 4.

The lithospheric temperature changes have a complex relationship to the surface displacements as well as to the temperature dependence of thermal conductivity and diffusivity. For instance, higher surface heat flow and hotter geotherms result in more subsidence and a higher surface temperature, but not necessarily greater Moho temperature changes (cf. models A1b and D9b). We find that increasing or decreasing the linear orogen temperature gradient by 10 K km^{-1} changes ΔT_c proportionately

Table 4. Thermal–mechanical model results.

Model	ΔT_c^{max} (K)	ΔT_c^{ε} (K)	F_o (TN m^{-1})	w_0 (km)	ε_e^c (per cent)	$\overline{h_e}$ (km)	h_e^{min} (km)	$-\Delta h_e^{min}$ (per cent)	Fig.
A1b	25	18	40	5.5	0.20	106	96	3	8
A2b	95	79	158	17.5	1.7	82	63	11	
D1b	11	5	5.2	1.4	2.1	56	41	11	6
D2b	30	14	18	5.1	12	37	28	17	6
D3b	63	31	37	10.5	26	26	17	42	6, 8
D4b	104	49	56	14.2	35	19	5	82	6, 7, 10
D5b	1	0	1.5	0.33	0.09	77	47	0	9
D6b	7	3	9.5	2.3	3.4	55	42	2	9
D7b	22	9	29	7.2	14	39	31	9	9
D8a	23	11	52	11.3	21	33	24	15	
D8b	46	20	53	11.9	23	30	20	28	5, 7, 9, 10
D8c	68	30	53	12.2	24	28	18	35	
D9b	20	7	50	10.6	17	38	29	12	7, 8, 10
F1b	104	56	47	16.9	77	3	0	0	8

For all models $\nabla T_o = 20$ K km^{-1}, except D8a and D8c for which $\nabla T_o = 10$ and 30 K km^{-1}, respectively.

(cf. models D8a–c). A heat transfer model with a constant thermal diffusivity of 10^{-6} m^2 s^{-1} (but temperature-dependent conductivity) produces differences of less than 5 K in ΔT_c.

These models reveal an important sensitivity of temperature changes at the Moho to convergence rate (Fig. 7). For a given load size (i.e. a particular x_o), more time has elapsed at slow convergence rates, allowing greater heating of the lower crust. Comparison of models D4b, D8b, and D9b indicates that ΔT_c scales roughly with the inverse of v.

Another significant feature of these models is the spatial offset between the maximum Moho temperature change and the maximum creep strain zone in the lower crust. Creep strains accommodate flexural shear stresses, which are greatest where the plate experiences the most bending (Brown & Phillips 2000). The maximum crustal creep strain is located beneath the load at $x \approx (0.5\text{–}0.8)x_o$ (Figs 6 and 7), regardless of whether a continuous or broken plate boundary condition applies. The ability of crustal heating beneath the orogen to modify the flexural response depends on the temperature change at this location, not at $x = 0$. These models show that ΔT_c^{ε} is generally only 40–60 per cent of ΔT_c^{max} (Table 4).

3.3.2 *Mechanics*

Figs 8–10 depict the effects of an evolving temperature field on the surface displacements and effective elastic thickness of the lithosphere. Here we compare $w(x)$ and $h_e(x)$ to the equivalent purely mechanical EVP models (Section 3.2); the parameter Δh_e^{min} equals the per cent change in $h_e(x)$ at $x = 0$. The thermal–mechanical model characteristics are provided in Table 4, to be compared to Table 3.

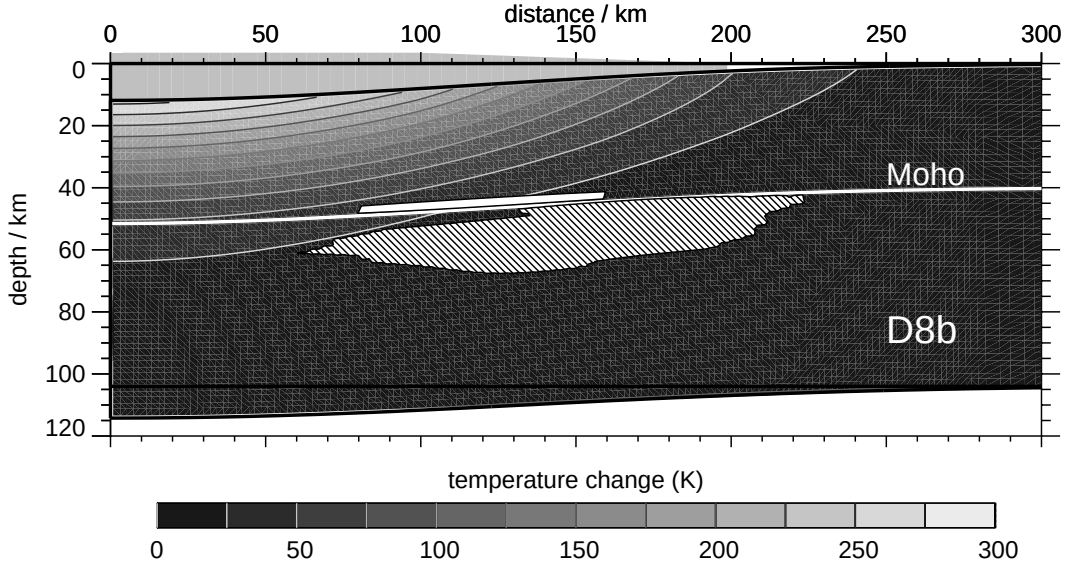

Figure 5. Contoured temperature changes in the crust and mantle of model D8b at 40 Myr. The orogenic wedge is depicted with the uniform grey shading at top. Elevated temperatures caused by lithospheric subsidence beneath the wedge are referenced to the initial steady-state geotherm. The oblong white zone in the lower crust marks the area of equivalent creep strains (ε_e^c) of at least 20 per cent. The cross-hatched zone in the upper mantle fills the area of shear stresses (σ_{xy}) exceeding 50 MPa. The temperature increase in this region of maximum deformation is small, ~20 K.

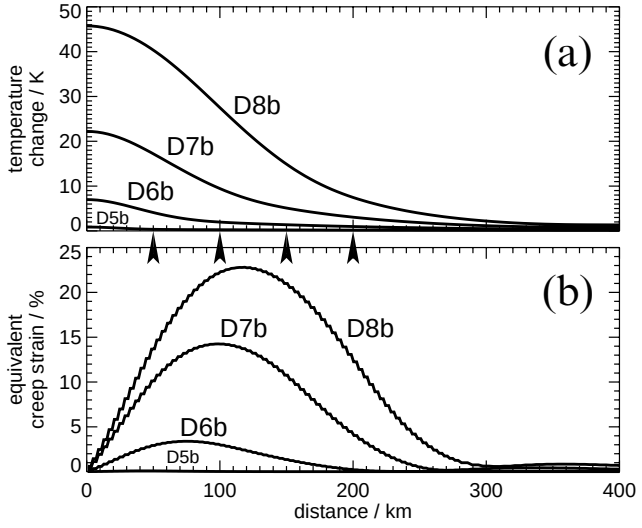

Figure 6. Thermal–mechanical model results at different times for the same initial geotherm (45 mW m^{-2}) and convergence rate (5 mm $year^{-1}$). (a) Temperature change at the Moho. (b) Equivalent creep strain at the base of the crust. Arrows mark the location of the orogenic wedge toe at each time step. Models D5–8b correspond to times of 10, 20, 30, and 40 Myr; see Table 4.

The lithospheric geotherm has only a modest influence on the change in the flexural signature, everything else being equal (Fig. 8). Warmer lithosphere experiences a somewhat greater increase in surface deflections than cooler lithosphere (compare models F1b to D3b and D9b to A1b). Likewise, hotter geotherms correspond to relatively greater decreases in the effective elastic thickness. Variations in the orogen temperature gradient produce much smaller changes in the surface deflections and effective elastic thicknesses than in Moho temperatures (cf. models D8a–c). With time and a growing load, the flexural changes relative to a purely mechanical model increase (Fig. 9). These results imply decreases in the effective elastic thickness of up to 80 per cent with 200 km of convergence (model D4b).

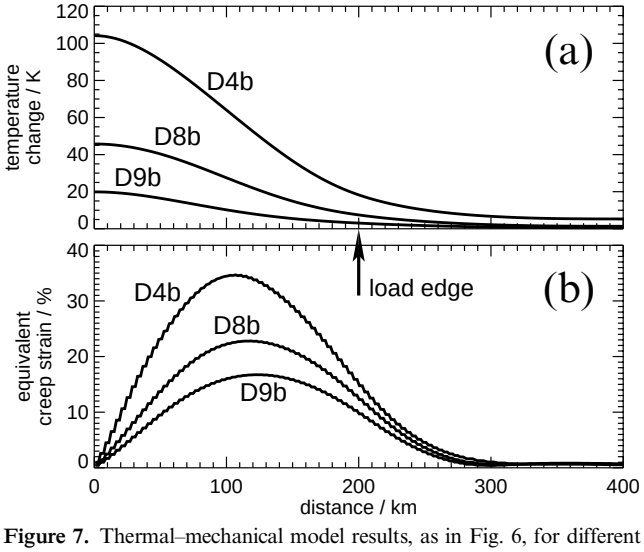

Figure 7. Thermal–mechanical model results, as in Fig. 6, for different orogenic convergence rates but the same initial geotherm and load position. Models D4b, D8b, and D9b have convergence rates of 2, 5, and 10 mm $year^{-1}$. Note the drop-off in ΔT_c at the location of maximum creep strain.

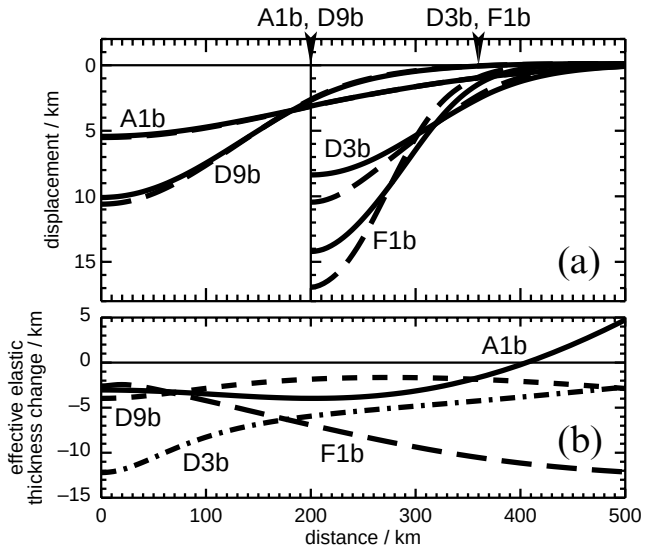

Figure 8. Thermal–mechanical flexural results for different initial geotherms; compare Fig. 3. (a) Vertical surface displacements. The solid curves are identical to those in Fig. 3(a); the long-dashed lines are for the thermal–mechanical solution. Note D3b and F1b have been offset 200 km for clarity. (b) Changes in the laterally variable effective elastic thickness relative to the purely mechanical models. See Table 4.

Because the convergence rate so strongly modulates temperature changes in the lower crust, this variable also exerts a controlling influence on the temperature-induced changes in flexure (Fig. 10). At the slowest convergence rate (2 mm $year^{-1}$), h_e^{min} drops 82 per cent from 25 to 5 km (model D4b). However, a more rapidly advancing orogen (10 mm $year^{-1}$) promotes only a minor, 12 per cent change in h_e^{min} (32 to 29 km, model D9b). Other models with 10 mm $year^{-1}$ convergence rates (e.g. A1b and A2b) support this finding.

We also examine a scenario in which the orogeny ceases and the crust continues to heat up with a constant, stationary applied load (Table 5). This situation results in a large decrease

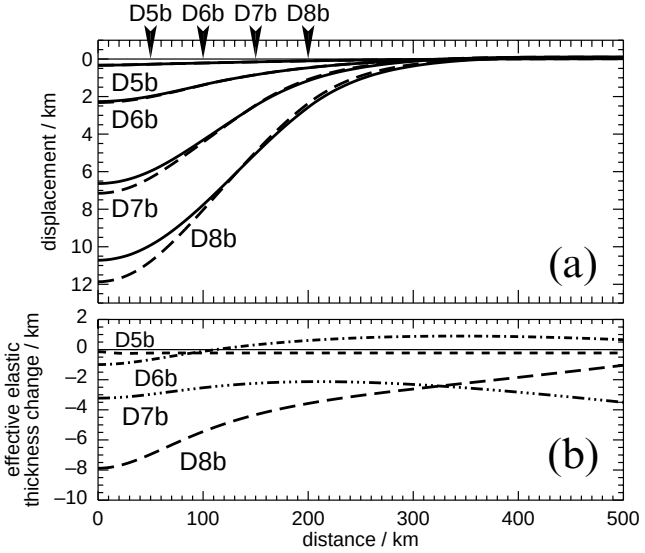

Figure 9. Thermal–mechanical flexural results, as in Fig. 8, at different times but for the same initial geotherm (45 mW m^{-2}) and loading rate (5 mm $year^{-1}$). Compare Fig. 4.

Table 5. Cessation of convergence.

Model	t (Myr)	ΔT_c^{max} (K)	ΔT_c^{ε} (K)	w_0 (km)	x_b (km)	ε_e^c (per cent)	$\overline{h_e}$ (km)
D8	40	—	—	10.7	304	18	36
D8b	40	46	20	11.9	296	23	30
D8d	45	67	35	12.0	216	26	23
D8e	50	80	45	12.1	188	27	17
D8f	55	92	54	12.2	168	28	11
D8g	60	102	62	12.2	160	29	9

in $\overline{h_e}$ from 29 km to 9 km for model D8b after 20 Myr of postloading evolution; $\overline{h_e}$ changes little thereafter. About one-third or more of this reduction is attributable just to stress relaxation (Brown & Phillips 2000); the remainder is thermal weakening. Note that the foreland basin width, as measured by the distance from the wedge toe to the crest of the flexural bulge (x_b), is reduced by almost 50 per cent. Narrowing and erosion of the basin would be readily apparent in the stratigraphy (e.g. Quinlan & Beaumont 1984) and could corroborate an anomalously low postorogenic effective elastic thickness.

4 DISCUSSION AND CONCLUSIONS

4.1 Steady-state geotherms and continental flexure

Our thermal modelling closely follows the analysis of Rudnick *et al.* (1998), and our results largely agree with theirs. Incorporating the temperature dependence of granulite thermal conductivity allows a somewhat higher average Archean crustal heat production than they needed to match xenolith geothermobarometry data. We have focused on the importance of the range of surface heat flows, the uncertain partitioning of heat producing elements into the crust, and the temperature dependence of crust and mantle thermal conductivity for Precambrian lithospheric geotherms, especially Moho temperatures. These results are summarized in Table 2 and Fig. 2(b).

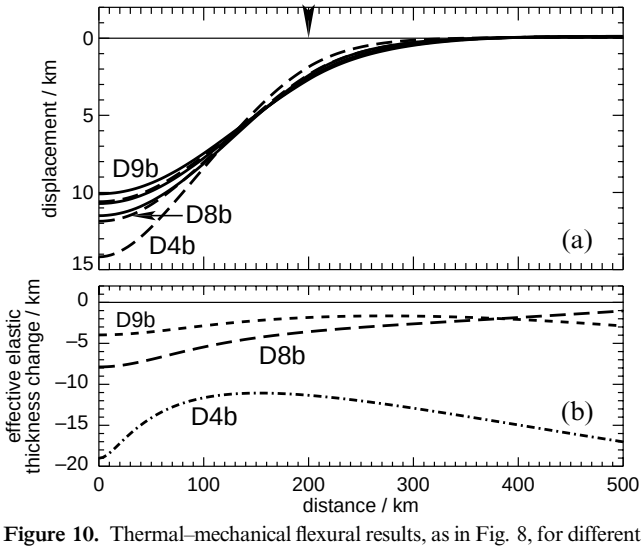

Figure 10. Thermal–mechanical flexural results, as in Fig. 8, for different loading rates but the same initial geotherm and load position. Also see Fig. 7. The decrease in effective elastic thickness is significant only for the slowest convergence rate (model D4b, 2 mm year^{-1}).

Although it is difficult to separate the effects of variations in crustal heat production and thermal conductivity in published continental geotherms, we can nonetheless make some useful comparisons. Most workers assume a single, unique partitioning of crustal heat production, often decreasing exponentially with depth. The equivalent average crustal heat generation (A_c) is in some cases realistic ($\sim$0.5–0.8 μW m^{-3}) and in others not ($\sim$2 μW m^{-3} (Batt & Braun 1997; Pope & Willet 1998)). Such assumptions neglect the large uncertainty in and variability of crustal heat production predicted by geochemical models of crustal composition and measurements of exposed crustal cross-sections (McLennan & Taylor 1996; Rudnick *et al.* 1998). Our models demonstrate that, for purposes of characterizing Moho temperatures, this uncertainty is at least as important as the range of Precambrian surface heat flow measurements.

For given values of q_0 and A_c, many published geotherms underestimate lower crustal temperatures compared to our results, by more than 100 K in some examples (Turcotte & Schubert 1982; Kusznir & Park 1986; Burov & Diament 1995; Midgley & Blundell 1997; Brown & Phillips 2000). (This comparison accounts for differences in crustal thickness, which is also significant.) These relatively low Moho temperatures from the literature are a consequence of the neglect of temperature- and depth-dependent thermal conductivity. Conductivity decreases with increasing temperatures, raising the temperature gradient for a given heat flux. Assumed exponential partitioning of crustal heat-producing elements also underrepresents lower crustal heat generation (with respect to the estimates of Rudnick & Fountain 1995), yielding lower temperatures at the Moho.

One might argue that the combination of scatter in surface heat flow, poorly constrained crustal heat production, and use of empirical thermal conductivity (which cannot replicate conductivity in the complex, heterogeneous continental crust) defeats any attempt to accurately characterize lower crustal temperatures. Indeed, carefully considering a range of either q_0 or A_c alone may be adequate to bracket T_c for modelling purposes. The important conclusion here is that a hot lower crust ($\sim$800 K) is entirely consistent with experimental thermal conductivity data and our understanding of Precambrian crustal composition.

The flexural implications of these thermal modelling results are illustrated by mechanical models E2 and F1 (Table 3, Fig. 3). The deformation of a 'hot', but realistic, Precambrian continental lithospheric plate by an orogenic load yields effective elastic thicknesses of $\sim$10 km. This finding immediately eliminates the paradox of anomalously low Precambrian elastic plate thicknesses at foreland basins, which has been a subject of concern for many authors (Watts 1992; Burov & Diament 1995; Lavier & Steckler 1997; Stewart & Watts 1997; Brown & Phillips 2000).

We postulate that the large range of effective elastic thicknesses determined for Proterozoic forelands ($\sim$100 km for the Himalayas to as low as 10 km for the Carpathians and the Andes) can be fully explained by spatial diversity in the compositional, thermal, and rheological properties of continental lithosphere. Precambrian lithosphere cannot be considered uniform in any of these properties. The complex genesis of continental crust allows for a multitude of regional and vertical compositional permutations that directly affect heat generation, thermal conductivity, and plastic creep of rocks. Heat flow from beneath the continental crust probably has spatial variations of

Table 6. Orogenic convergence rate estimates.

Location	Time	Method	Rate (mm yr^{-1})	Reference
Antler orogeny, Nevada	Palaeozoic	conodont biostratigraphy	>6	Johnson & Pendergast (1981)
Taconic orogeny, Appalachians, eastern United States	Ordovician	graptolite biostratigraphy	10–40	Bradley & Kusky (1986); Bradley (1989); Finney *et al.* (1996)
North American Cordillera, Idaho–Wyoming and southern Canada	Mesozoic–Cenozoic	crustal thickening	2	Jordan *et al.* (1988)
Central Precordillera and Subandes, Argentina	Neogene	crustal thickening, thrust fault displacements and ages	>5	Jordan *et al.* (1988, 1993)
Central Precordillera and Subandes, Bolivia	Cenozoic	balanced cross sections	>3	Sheffels (1990)
central Andes, Bolivia	present	GPS, modelling	<40	Liu *et al.* (2000)
Himalayas, India	Neogene	foreland basin stratigraphy	10–15	Lyon-Caen & Molnar (1985)
Carpathians, Romania	Late Miocene–present	restored cross sections	15–20	Linzer *et al.* (1998)
southern Tien Shan, China	Quaternary	restored cross sections	3–21	Burchfiel *et al.* (1999)
Tien Shan, Kyrgyzstan and Kazakhstan	present	GPS	~10	Abdrakhmatov 1996)

~ 10 mW m^{-2} as well (Morgan 1984). The magnitude and distribution of loads play a secondary, though very important, role in the flexural response, but crust–mantle decoupling is essential to our explanation of Precambrian effective elastic thicknesses.

4.2 Thermal–mechanical evolution of foreland lithosphere

Although the substantial uncertainty in crustal heat production can explain the ~10–100 km range in mountain belt effective elastic thicknesses, we have also proceeded to analyse the consequences of foreland thermal evolution beneath the orogen. We maximize the thermal weakening of the crust by overestimating the orogen's linear temperature gradient. The temperature dependence of thermal diffusivity has only a small effect on the results, but it is included. Models are run to 200 km of convergence because flexural observations indicate that generally no more than this length of underthrust plate supports the orogen.

Figs 5, 7, and 10 illustrate the fundamental results of the thermal–mechanical modelling. The flexural response to heating of the lithosphere is most sensitive to temperature changes near the Moho, where the rheological contrast between weak lower crust and strong upper mantle produces crust–mantle decoupling. Maximum Moho temperature increases vary inversely with loading rate and can be quite large (~100 K). However, the temperature change where flexural shear stresses are relaxed and decoupling is localized (in between the plate edge and the wedge toe) is only about half as great. Hence, the decrease in effective elastic thickness is significant (i.e. changing at least ~30 per cent for $x_o \leq 200$ km) only for slow orogenic convergence rates of ≤ 5 mm $year^{-1}$ (models D4b, D8b).

Given the importance of convergence rate to the flexural response, what are typical convergence or shortening rates for continental orogens? Although these are difficult parameters to determine, estimates have been published for several mountain belts. Convergence rates must be greater than shortening rates because both structural deformation and wholesale underthrusting accommodate convergence. Table 6 summarizes orogenic convergence rates from the literature.

These representative continental convergence rates of ~5–20 mm $year^{-1}$ are much less than oceanic subduction rates of ~25–85 mm $year^{-1}$ (Jarrard 1986). Nevertheless, they are generally too fast for the lower crust of the advecting foreland lithosphere to be thermally influenced by the overriding orogen. If convergence ceases, the crust continues to heat up and the lithospheric flexural rigidity will rapidly decrease (to ~10 km for model D8b). However, the forelands exhibiting anomalously low effective elastic thicknesses occur at presently or very recently active orogens such as the Andes, Carpathians, and Tien Shan. (Possibly convergence in the eastern Carpathians ended in the Late Miocene (Sandulescu 1988), but there is evidence for contractional deformation continuing into the Pliocene (Linzer *et al.* 1998). We conclude that the thermal evolution of foreland lithosphere at active orogens is of only minor importance to its flexural evolution, contrary to the assessment of Lavier & Steckler (1997). We reiterate that the large range of continental effective elastic thickness estimates can be fully explained by the variability of heat flow and heat production in Precambrian crust.

ACKNOWLEDGMENTS

I thank Roger Phillips for his support of this work. An anonymous reviewer's thorough commentary greatly improved the manuscript. The research described here was supported by NSF grant EAR-9706140.

REFERENCES

Abdrakhmatov, K.Ye *et al.*, 1996. Relatively recent construction of the Tien Shan inferred from GPS measurements of present-day crustal deformation rates, *Nature,* **384,** 450–453.

Arndt, J., Bartel, T., Scheuber, E. & Schilling, F., 1997. Thermal and rheological properties of granodioritic rocks from the Central Andes, north Chile, *Tectonophysics,* **271,** 75–88.

Batt, G.E. & Braun, J., 1997. On the thermomechanical evolution of compressional orogens, *Geophys. J. Int.,* **128,** 364–382.

Blackwell, D.D., 1971. The thermal structure of the continental crust, in *The Structure and Physical Properties of the Earth's Crust,* pp. 169–184, ed. by Heacock, J.G., American Geophysical Union, Washington, DC.

Bradley, D.C., 1989. Taconic plate kinematics as revealed by foredeep stratigraphy, Appalachian orogen, *Tectonics,* **8,** 1037–1049.

Bradley, D.C. & Kusky, T.M., 1986. Geologic evidence for rate of plate convergence during the Taconic arc-continent collision, *J. Geol.,* **94,** 667–681.

Brown, C.D. & Phillips, R.J., 2000. Crust–mantle decoupling by flexure of continental lithosphere, *J. geophys. Res.,* **105,** 13,221–13,237.

Burchfiel, B.C., Brown, E.T., Deng Qidong, FengXianyue, Li June, Molnar, P., Shi Jianbang, Wu Zhangming & You Huichuan, 1999. Crustal shortening on the margins of the Tien Shan, Xinjiang, China, *Int. Geol. Rev.,* **41,** 665–700.

Burov, E.B. & Diament, M., 1995. The effective elastic thickness (T_e) of continental lithosphere: What does it really mean?, *J. geophys. Res.,* **100,** 3905–3927.

Chapman, D.S., 1986. Thermal gradients in the continental crust, in *The Nature of the Lower Continental Crust*, pp. 63–70, ed. Dawson, J.B. *et al.*, *Geol Society Spec. Pubs*, 24 Blackwell, Oxford.

Chery, J., Vilotte, J.P. & Daignieres, M., 1991. Thermomechanical evolution of a thinned continental lithosphere under compression: Implications for the Pyrenees, *J. geophys. Res.,* **96,** 4385–4412.

Chopra, P.N. & Paterson, M.S., 1981. The experimental deformation of dunite, *Tectonophysics,* **78,** 453–473.

Christensen, N.I. & Mooney, W.D., 1995. Seismic velocity structure and composition of the continental crust: a global view, *J. geophys. Res.,* **100,** 9761–9788.

Clauser, C. *et al.*, 1997. The thermal regime of the crystalline continental crust: Implications from the KTB, *J. geophys. Res.,* **102,** 18,417–18,441.

Clauser, C. & Huenges, E., 1995. Thermal conductivity of rocks and minerals, in *Rock Physics and Phase Relations: a Handbook of Physical Constants,* pp. 105–126, ed. Ahrens, T.J., American Geophysical Union, Washington, DC.

Demetrescu, C. & Andreescu, M., 1994. On the thermal regime of some tectonic units in a continental collision environment in Romania, *Tectonophysics,* **230,** 265–276.

Doin, M.P. & Fleitout, L., 1996. Thermal evolution of the oceanic lithosphere, An Alternative View, *Earth planet. Sci. Lett.,* **142,** 121–136.

Drury, M.J., 1989. The heat flow–heat generation relationship: implications for the nature of continental crust, *Tectonophysics,* **164,** 93–106.

Durham, W.B., Mirkovich, V.V. & Heard, H.C., 1987. Thermal diffusivity of igneous rocks at elevated pressure and temperature, *J. geophys. Res.,* **92,** 11,615–11,634.

Finney, S.C., Grubb, B.J. & Hatcher, R.D., 1996. Graphic correlation of Middle Ordovician graptolite shale, southern Appalachians: an approach for examining the subsidence and migration of a Taconic foreland basin, *Bull. geol. Soc. Am.,* **108,** 355–371.

Fountain, D.M., Furlong, K.P. & Salisbury, M.H., 1987. A heat production model of a shield area and its implications for the heat flow–heat production relationship, *Geophys. Res. Lett.,* **14,** 283–286.

Furlong, K.P. & Chapman, D.S., 1987. Crustal heterogeneities and the thermal structure of the continental crust, *Geophys. Res. Lett.,* **14,** 314–317.

Gillet, P., Richet, P., Guyot, F. & Fiquet, G., 1991. High-temperature thermodynamic properties of forsterite, *J. geophys. Res.,* **96,** 11,805–11,816.

Gupta, M.L., 1993. Is the Indian Shield hotter than other Gondwana shields?, *Earth planet. Sci. Lett.,* **115,** 275–285.

Hansen, F.D. & Carter, N.L., 1983. Semibrittle creep of dry and wet Westerly granite at 1000 MPa, *US Symp Rock Mechanics,* **24,** 429–447.

Henry, P., Le Pichon, X. & Goffé, B., 1997. Kinematic, thermal and petrological model of the Himalayas: Constraints related to metamorphism within the underthrust Indian crust and topographic elevation, *Tectonophysics,* **273,** 31–56.

Henry, S.G. & Pollack, H.N., 1988. Terrestrial heat flow above the Andean subduction zone in Bolivia and Peru, *J. geophys. Res.,* **93,** 15,153–15,162.

Hofmeister, A.M., 1999. Mantle values of thermal conductivity and the geotherm from phonon lifetimes, *Science,* **283,** 1699–1706.

Huerta, A.D., Royden, L.H. & Hodges, K.V., 1998. The thermal structure of collisional orogens as a response to accretion, erosion, and radiogenic heating, *J. geophys. Res.,* **103,** 15,287–15,302.

Jarrard, R.D., 1986. Relations among subduction parameters, *Rev. Geophys.,* **24,** 217–284.

Jessop, A.M., 1990. *Thermal Geophysics,* Developments in Solid Earth Geophysics, 17, Elsevier, New York.

Johnson, J.G. & Pendergast, A., 1981. Timing and mode of emplacement of the Roberts Mountains allochthon, Antler orogeny, *Bull. geol. Soc. Am.,* **92,** 648–658.

Jordan, T.E., Allmendinger, R.W., Damanti, J.F. & Drake, R.E., 1993. Chronology of Motion in a Complete Thrust Belt: the Precordillera, 30–31°S, Andes Mountains, *J. Geology,* **101,** 135–156.

Jordan, T.E., Flemings, P.B. & Beer, J.A., 1988. Dating thrust-fault activity by use of foreland-basin strata, in *New Perspectives in Basin Analysis*, pp. 307–330, ed. Kleinspehn, K.L. & Paola, C., Springer-Verlag, New York.

Karner, G.D., 1991. Sediment blanketing and the flexural strength of extended continental lithosphere, *Basin Res.,* **3,** 177–185.

Karner, G.D. & Watts, A.B., 1983. Gravity anomalies and flexure of the lithosphere at mountain ranges, *J. geophys. Res.,* **88,** 10,449–10,477.

Ketcham, R.A., Beam, E.C. & Kominz, M.A., 1995. Effects of temperature-dependent material properties and radioactive heat production on simple basin subsidence models, *Earth planet. Sci. Lett.,* **130,** 31–44.

Kremenetsky, A.A., Milanovsky, S.Yu & Ovchinnikov, L.N., 1989. A heat generation model for continental crust based on deep drilling in the Baltic Shield, *Tectonophysics,* **159,** 231–246.

Kusznir, N.J. & Park, R.G., 1986. Continental lithosphere strength: The critical role of lower crustal deformation, in *The Nature of the Lower Continental Crust,* pp. 79–93, ed. Dawson, J.B. *et al.*, Geol, Society Spec. Pubs, 24, Blackwell, Oxford.

Lavier, L.L. & Steckler, M.S., 1997. The effect of sedimentary cover on the flexural strength of continental lithosphere, *Nature,* **389,** 476–479.

Lenardic, A., 1997. On the heat flow variation from Archean cratons to Proterozoic mobile belts, *J. geophys. Res.,* **102,** 709–721.

Linzer, H.-G., Frisch, W., Zweigel, P., Girbacea, R., Hann, H.-P. & Moser, F., 1998. Kinematic evolution of the Romanian Carpathians, *Tectonophysics,* **297,** 133–156.

Liu, M., Yang, Y., Stein, S., Zhu, Y. & Engeln, J., 2000. Crustal shortening in the Andes: why do GPS rates differ from geological rates?, *Geophys. Res. Lett.,* **27,** 3005–3008.

Lyon-Caen, H. & Molnar, P., 1983. Constraints on the structure of the Himalaya from an analysis of gravity anomalies and a flexural model of the lithosphere, *J. geophys. Res.,* **88,** 8171–8191.

Lyon-Caen, H. & Molnar, P., 1985. Gravity anomalies, flexure of the Indian plate, and the structure, support and evolution of the Himalaya and Ganga Basin, *Tectonics,* **4,** 513–538.

Lyon-Caen, H., Molnar, P. & Saurez, G., 1985. Gravity anomalies and flexure of the Brazilian Shield beneath the Bolivian Andes, *Earth planet. Sci. Lett.,* **75,** 81–92.

Maţenco, L., Zoetemeijer, R., Cloetingh, S. & Dinu, C., 1997. Lateral variations in mechanical properties of the Romanian external Carpathians: inferences of flexure and gravity modelling, *Tectonophysics,* **282,** 147–166.

McLennan, S.M. & Taylor, S.R., 1996. Heat flow and the chemical composition of continental crust, *J. Geol,* **104,** 369–377.

McNutt, M.K., Diament, M. & Kogan, M.G., 1988. Variations of elastic plate thickness at continental thrust belts, *J. geophys. Res.,* **93,** 8825–8838.

Mezger, K., 1992. Temporal evolution of regional granulite terranes: implications for the formation of lowermost continental crust, in *Continental Lower Crust,* pp. 447–478, ed. Fountain, D.M., Arculus, R. & Kay, R.W., Developments in Geotectonics, 23, Elsevier, New York.

Midgley, J.P. & Blundell, D.J., 1997. Deep seismic structure and thermo-mechanical modelling of continental collision zones, *Tectonophysics,* **273,** 155–167.

Molnar, P. & England, P., 1990. Temperatures, heat flux, and frictional stress near major thrust faults, *J. geophys. Res.,* **95,** 4833–4856.

Morgan, P., 1984. The thermal structure and thermal evolution of the continental lithosphere, in *Structure and Evolution of the Continental Lithosphere,* pp. 107–193, ed. Pollack, H.N. & Murthy, V.R., Physics and Chemistry of the Earth, 15, Pergamon, New York.

Mueller, S. & Phillips, R.J., 1995. On the reliability of lithospheric constraints derived from elastic models of outer-rise flexure, *Geophys. J. Int.,* **123,** 887–902.

Nyblade, A.A. & Pollack, H.N., 1993. A global analysis of heat flow from Precambrian terrains: Implications for the thermal structure of Archean and Proterozoic lithosphere, *J. geophys. Res.,* **98,** 12,207–12,218.

Pollack, H.N. & Chapman, D.S., 1977. On the regional variation of heat flow, geotherms, and lithospheric thickness, *Tectonophysics,* **38,** 279–296.

Pollack, H.N., Hurter, S.J. & Johnson, J.R., 1993. Heat flow from the Earth's interior: Analysis of the global data set, *Rev. Geophys.,* **31,** 267–280.

Pope, D.C. & Willet, S.D., 1998. Thermal-mechanical model for crustal thickening in the Central Andes driven by ablative subduction, *Geology,* **26,** 511–514.

Press, W.H., Teukolsky, S.A., Vetterling, W.T. & Flannery, B.P., 1992. *Numerical Recipes in C,* 2nd edn., Cambridge University Press, New York.

Quinlan, G.M. & Beaumont, C., 1984. Appalachian thrusting, lithospheric flexure, and the Paleozoic stratigraphy of the Eastern Interior of North America, *Can. J. Earth Sci.,* **21,** 973–996.

Roy, S. & Rao, R.U.M., 2000. Heat flow in the Indian shield, *J. geophys. Res.,* **105,** 25 587–25 604.

Royden, L.H., 1993a. The tectonic expression of slab pull at continental convergent boundaries, *Tectonics,* **12,** 303–325.

Royden, L.H., 1993b. The steady state thermal structure of eroding orogenic belts and accretionary prisms, *J. geophys. Res.,* **98,** 4487–4507.

Royden, L. & Karner, G.D., 1984. Flexure of lithosphere beneath Apennine and Carpathian foredeep basins: Evidence for an insufficient topographic load, *Am. Assoc. Petrol. Geol. Bull.,* **68,** 704–712.

Rudnick, R.L., 1992. Xenoliths—Samples of the lower continental crust. In: *Continental Lower Crust,* pp. 269–316, eds Fountain, D.M., Arculus, R. & Kay, R.W., Developments in Geotectonics, 23, Elsevier, New York.

Rudnick, R.L. & Fountain, D.M., 1995. Nature and composition of the continental crust: a lower crustal perspective, *Rev. Geophys.,* **33,** 267–309.

Rudnick, R.L., McDonough, W.F. & O'Connell, R.J., 1998. Thermal structure, thickness and composition of continental lithosphere, *Chem. Geol.,* **145,** 395–411.

Sandulescu, M., 1988. Cenozoic tectonic history of the Carpathians, in *The Pannonian Basin,* pp. 17–25, ed. Royden, L.H. & Horváth, F, American Association of Petroleum Geologists, Tulsa.

Sass, J.H., Lachenbruch, A.H., Moses, T.H. & Morgan, P., 1992. Heat flow from a scientific research well at Cajon Pass, California, *J. geophys. Res.,* **97,** 5017–5030.

Saxena, S.K. & Shen, G., 1992. Assessed data on heat capacity, thermal expansion, and compressibility for some oxides and silicates, *J. geophys. Res.,* **97,** 19 813–19 825.

Schatz, J.F. & Simmons, G., 1972. Thermal conductivity of earth materials at high temperatures, *J. geophys. Res.,* **77,** 6966–6983.

Seipold, U., 1998. Temperature dependence of thermal transport properties of crystalline rocks—a general law, *Tectonophysics,* **291,** 161–171.

Sheffels, B.M., 1990. Lower bound on the amount of crustal shortening in the central Bolivian Andes, *Geology,* **18,** 812–815.

Snyder, D.B. & Barazangi, M., 1986. Deep crustal structure and flexure of the Arabian plate beneath the Zagros collisional mountain belt as inferred from gravity observations, *Tectonics,* **5,** 361–373.

Springer, M. & Förster, A., 1998. Heat-flow density across the Central Andean subduction zone, *Tectonophysics,* **291,** 123–139.

Starin, L., Yuen, D.A. & Bergeron, S.Y., 2000. Thermal evolution of sedimentary basin formation with variable thermal conductivity, *Geophys. Res. Lett.,* **27,** 265–268.

Stephenson, R.A., Nakiboglu, S.M. & Kelly, M.A., 1989. Effects of asthenosphere melting, regional thermoisostasy, and sediment loading on the thermomechanical subsidence of extensional sedimentary basins, in *Origin and Evolution of Sedimentary Basins and Their Energy and Mineral Resources*, pp. 17–27, ed. Price, R.A., American Geophysical Union, Washington, DC.

Stewart, J. & Watts, A.B., 1997. Gravity anomalies and spatial variations of flexural rigidity at mountain ranges, *J. geophys. Res.,* **102,** 5327–5352.

Turcotte, D.L. & Schubert, G., 1982. *Geodynamics,* John Wiley, New York.

Watts, A.B., 1992. The effective elastic thickness of the lithosphere and the evolution of foreland basins, *Basin Res.,* **4,** 169–178.

Watts, A.B., Lamb, S.H., Fairhead, J.D. & Dewey, J.F., 1995. Lithospheric flexure and bending of the Central Andes, *Earth planet. Sci. Lett.,* **134,** 9–21.

Wilks, K.R. & Carter, N.L., 1990. Rheology of some continental lower crustal rocks, *Tectonophysics,* **182,** 57–77.

Zoetemeijer, R., Desegaulx, P., Cloetingh, S., Roure, F. & Moretti, I., 1990. Lithospheric dynamics and tectonic–stratigraphic evolution of the Ebro Basin, *J. geophys. Res.,* **95,** 2701–2711.

Zoth, G. & Haenel, R., 1988. Appendix, in *Handbook of Terrestrial Heat-Flow Density Determination,* pp. 449–466, eds Haenel, R., Rybach, L. & Stegena, L., Kluwar Academic, Boston.